Supporting Information

Construction of Chemically Self-Charging Aqueous Zinc Ion Batteries Based on Defect Coupled Nitrogen modulation of Zinc Manganite Vertical Graphene Arrays

Wenda Qiu,‡*[ab] Zhenchao Lin,‡[a] Hongbing Xiao,[a] Guoming Zhang,[a] Hong Gao,[a] Huajie Feng*[c] and Xihong Lu[b]

[a] *Guangdong Industry Polytechnic, 152 Xingang West Road, Guangzhou 510300, China.*

[b] *MOE of the Key Laboratory of Bioinorganic and Synthetic Chemistry, KLGHEI of Environment and Energy Chemistry, School of Chemistry, Sun Yat-Sen University, 135 Xingang West Road, Guangzhou 510275, China.*

[c] *Key Laboratory of Electrochemical Energy Storage and Energy Conversion of Hainan Province, School of Chemistry and Chemical Engineering, Hainan Normal University, Haikou 571158, China.*

Corresponding Author. E-mail: qiuwd3@mail3.sysu.edu.cn (W. Qiu); Fenghuajiehk@163.com (H. Feng).

‡Wenda Qiu and Zhenchao Lin contributed equally to this work.

Calculations:

The areal cell capacitances (C_{cell-a}) were calculated from the discharge curve using the following equations:

$$C_{cell-a} = \frac{\int_0^{\Delta t} I \times dt}{S}$$

(1)

where I (mA) is the applied discharging current, Δt (h) is the discharging time and S (cm^2) is the area of cell (0.5 cm^2).

Specific capacities (C_{cell-s}) of the cell were estimated from the discharge curve using the following equations:

$$C_{cell-s} = \frac{\int_0^{\Delta t} I \times dt}{m}$$

(2)

where C_{cell-s} (mA h g^{-1}) is the specific capacity of the H-ZMO NTAs//Zn battery, I (mA) is the applied discharging current, Δt (h) is the discharging time and m (g) is the mass of the active material of H-ZMO NTAs (3.2 mg cm^{-2}).

Specific energy density E and specific power density P of the cell were obtained from the following equations:

$$E = C_{cell-s} * \Delta V$$

(3)

$$P = \frac{C_{cell-s} * \Delta V}{1000 * \Delta t}$$

(4)

where E (Wh kg^{-1}) is the energy density, C_{cell-s} is the specific capacity obtained from Equation (2) and ΔV (V) is the voltage window. P (kW kg^{-1}) is the specific power density and Δt (h) is the discharging time.

The chemical diffusion coefficient of Zn^{2+} can be calculated based on the following equation:

$$D_{GITT} = \frac{4}{\pi \tau} \left(\frac{n_m V_m}{s}\right)^2 \left(\frac{\Delta E_s}{\Delta E_t}\right)^2$$

(5)

Here, τ (s) is the duration of the current pulse; n_m (mol) is the number of moles; V_m (cm^3 mol^{-1}) is the molar volume of the electrode; S (cm^2) is the electrode/electrolyte contact area; ΔE_s is the steady state voltage change due to the current pulse, and ΔE_t is the voltage change during the constant current pulse, eliminating the iR drop.
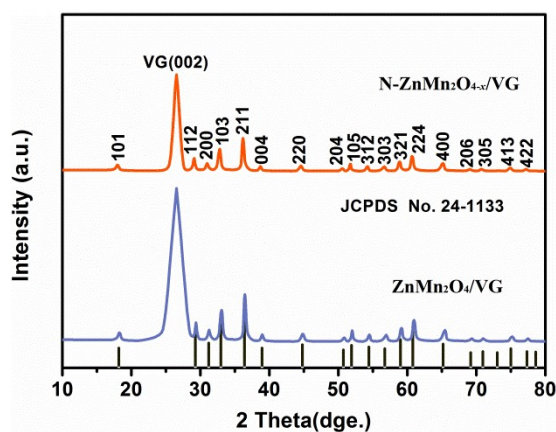
Figure S1. XRD patterns of ZnMn$_2$O$_4$/VG and N-ZnMn$_2$O$_{4-x}$/VG.
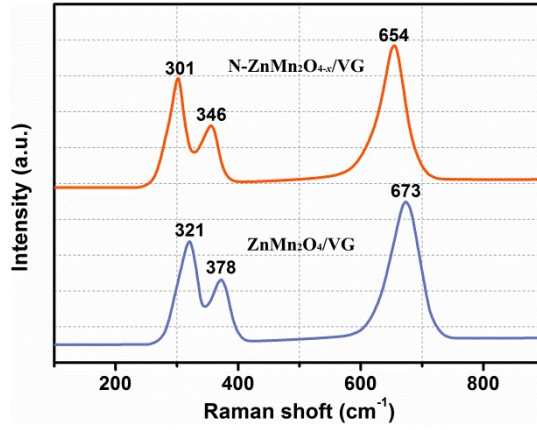
Figure S2. Raman spectra of $ZnMn_2O_4/VG$ and $N\text{-}ZnMn_2O_{4\text{-}x}/VG$.
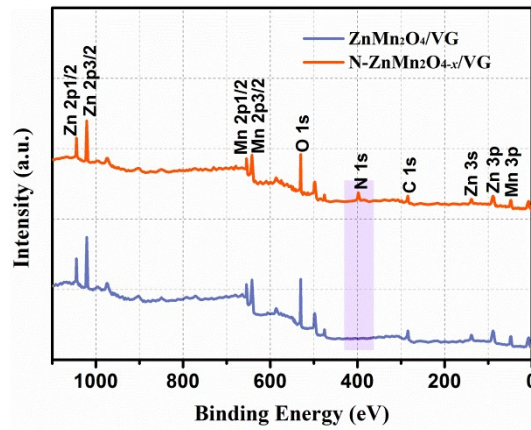
Figure S3. XPS survey spectra of $ZnMn_2O_4/VG$ and $N\text{-}ZnMn_2O_{4\text{-}x}/VG$.
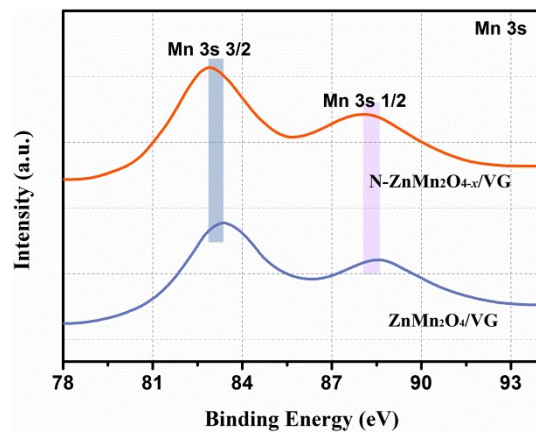
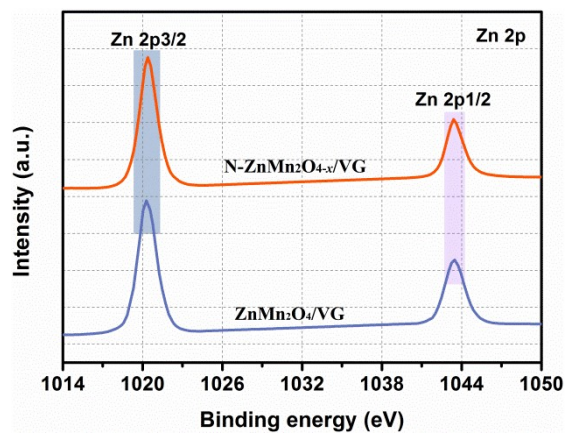Figure S4. Core-level Mn 3s XPS spectra of $ZnMn_2O_4$/VG and N-$ZnMn_2O_{4-x}$/VG.

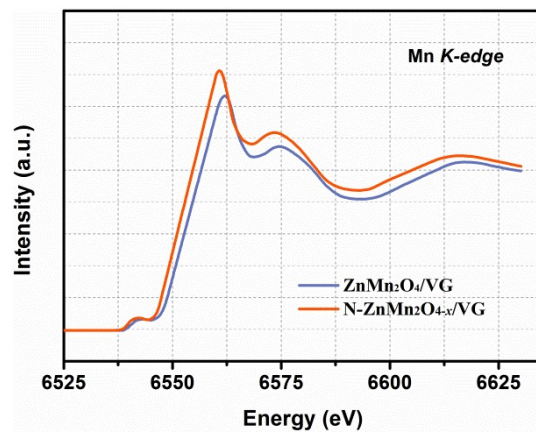Figure S5. Core-level Zn 2p XPS spectra of $ZnMn_2O_4$/VG and N-$ZnMn_2O_{4-x}$/VG.

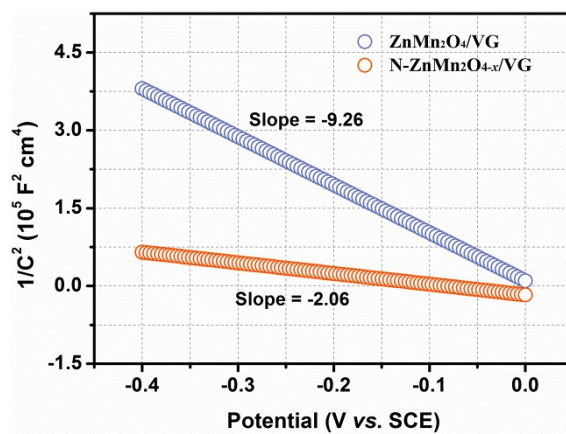Figure S6. Mn K-edge XPS spectra of $ZnMn_2O_4$/VG and N-$ZnMn_2O_{4-x}$/VG.

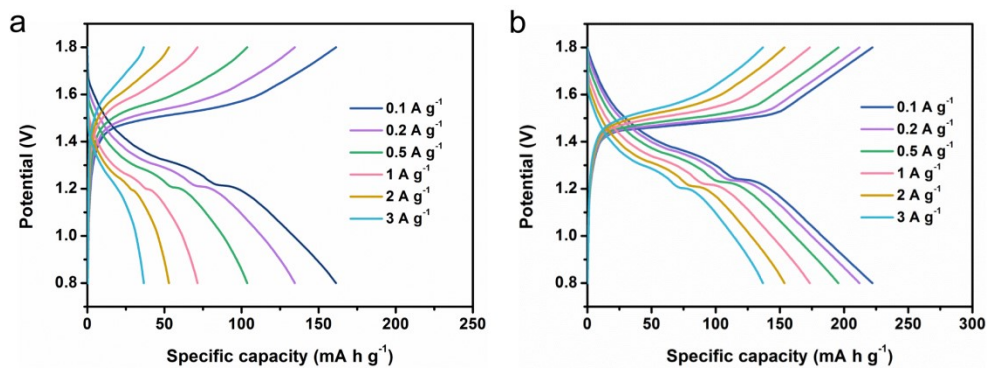Figure S7. Mott−Schottky plots of $ZnMn_2O_4$/VG and N-$ZnMn_2O_{4-x}$/VG.

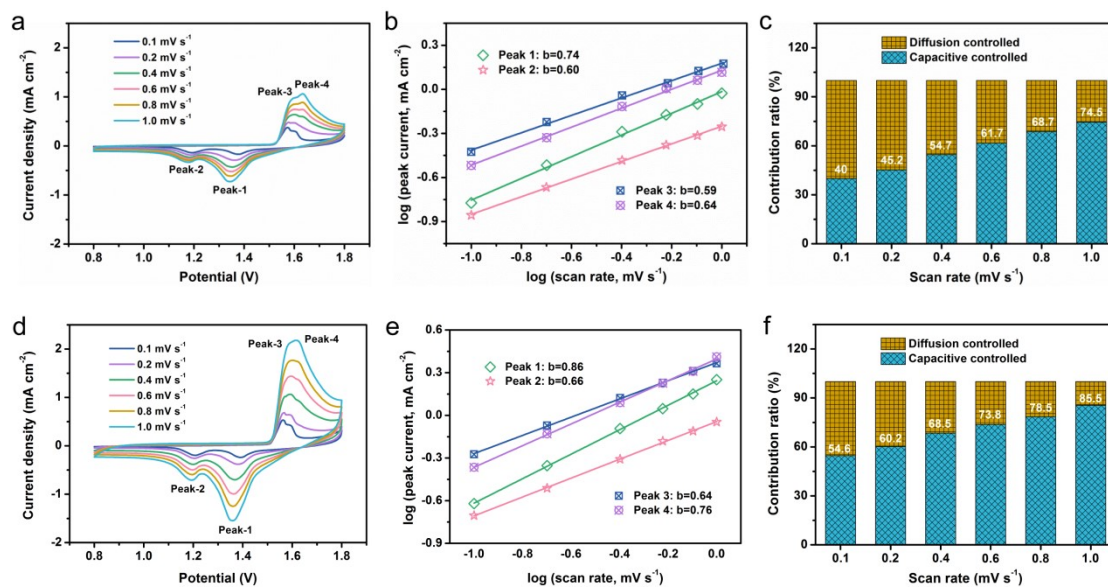Figure S8. GCD curves of the (a) ZnMn$_2$O$_4$/VG and (b) N-ZnMn$_2$O$_{4-x}$/VG batteries.

Figure S9. (a) CV curves, (b) log (*i*) *vs*. log (*v*) at each peak in (a), and (c) surface

capacitive contribution of the ZnMn$_2$O$_4$/VG electrode. (d) CV curves, (e) log (i) $vs.$ log (v) at each peak in (e), and (f) surface capacitive contribution of the N-ZnMn$_2$O$_{4-x}$/VG electrode.
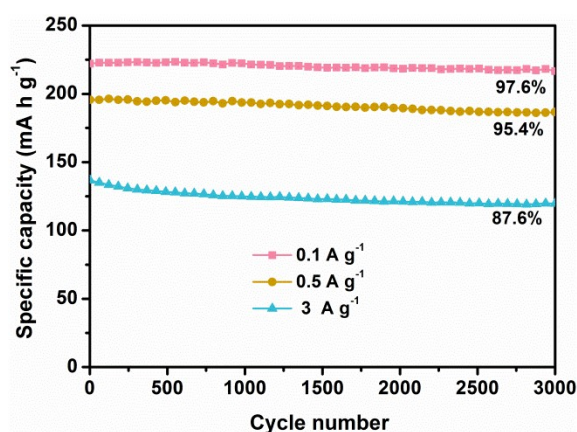

Figure S10. The cycling performance of N-ZnMn$_2$O$_{4-x}$/VG//Zn battery tested at 0.1, 0.5 and 3.0 A g^{-1}.
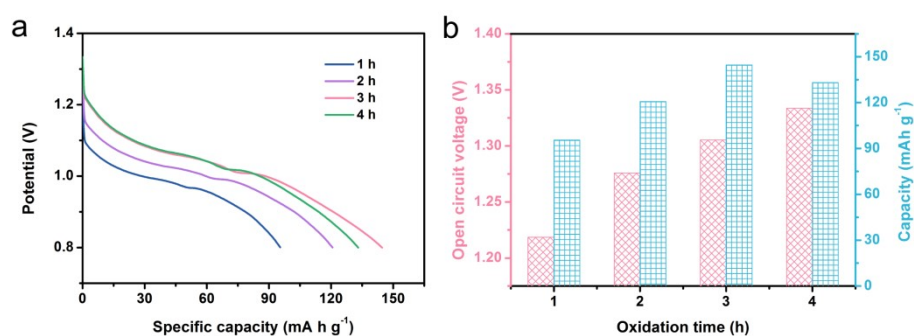
Figure S11. Electrochemical performance of N-Zn$_{1-x}$Mn$_2$O$_{4-x}$/VG//Zn batteries after the N-ZnMn$_2$O$_{4-x}$/VG electrodes are oxidized in deionized water for different times. (a) The galvanostatic discharge curves of N-Zn$_{1-x}$Mn$_2$O$_{4-x}$/VG//Zn batteries at 0.1 A g^{-1}. (b) Effect of the oxidation time on OCV and discharge capacity of N-Zn$_{1-x}$Mn$_2$O$_{4-x}$/VG//Zn batteries.
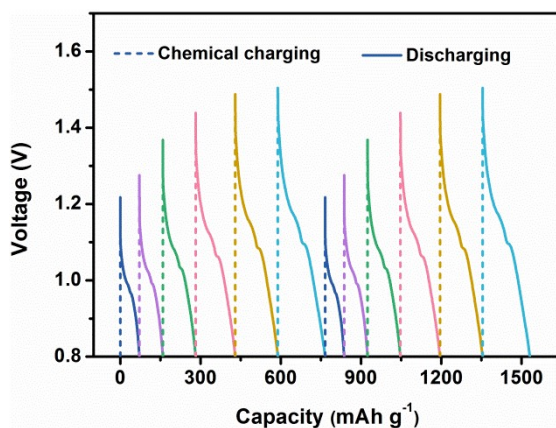
Figure S12. The chemical charging/galvanostatic discharging curves of N-Zn$_{1-x}$Mn$_2$O$_{4-x}$/VG//Zn batteries at different chemically charge states (dotted lines: chemical charging for different times. Solid lines: galvanostatic discharging at 0.1 A g^{-1}).
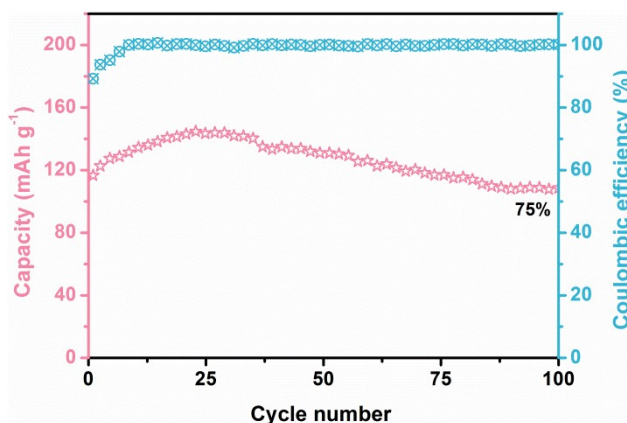

Figure S13. Cycle stability of N-Zn$_{1-x}$Mn$_2$O$_{4-x}$/VG//Zn battery at 0.1 A g^{-1} after the N-ZnMn$_2$O$_{4-x}$/VG electrode is oxidized in deionized water for 3 h.
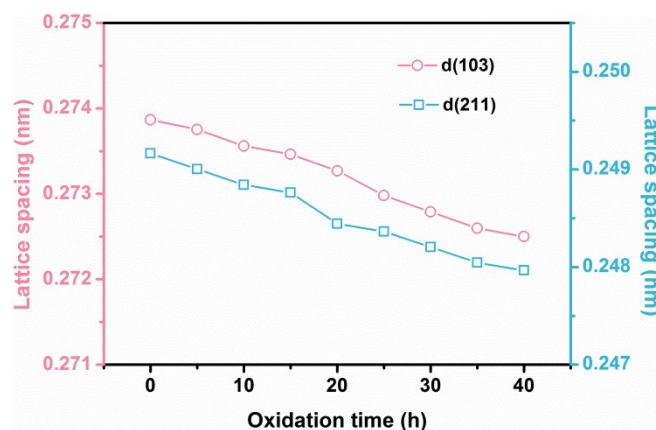
Figure S14. Calculational lattice spacing of (003) and (211) plane of N-ZnMn$_2$O$_{4-x}$/VG electrodes after being oxidized by O$_2$ for different times.

Table S1. Comparison of zinc storage performance of based cathodes.

Cathodes	Capacity (mA h g^{-1})	Rate performance	Cycling stability (cycles)	Ref.
N-ZnMn$_2$O$_{4-x}$/VG	222 (0.1 A g^{-1})	61.2% (0.1 to 3 A g^{-1})	97.6% (3000)	This work
ZnMn$_2$O$_4$ NDs/rGO	185 (0.1 A g^{-1})	60.5% (0.1 to 5 A g^{-1})	72.4% (400)	[1]
ZnO-MnO@C	219 (0.1 A g^{-1})	60.3% (0.1 to 3 A g^{-1})	84% (2000)	[2]
Hollow porous ZnMn$_2$O$_4$	112 (0.1 A g^{-1})	57% (0.1 to 3.2 A g^{-1})	No negligible	[3]
ZMO@Ti$_3$C$_2$T$_x$	172.6 (0.1 A g^{-1})	48.9% (0.1 to 4 A g^{-1})	92.4% (5000)	[4]

ZMO/C	150 (0.05 A g^{-1})	48% (0.05 to 2 A g^{-1})	94% (500)	[5]
ZMO@PCPs	177 (0.1 A g^{-1})	48% (0.1 to 4.0 A g^{-1})	90.3% (2000)	[6]
ZMO microrods	180 (0.1 A g^{-1})	47.8% (0.1 to 2.4 A g^{-1})	79% (3000)	[7]
ZMO	230 (0.5 A g^{-1})	43.9% (0.5 to 8 A g^{-1})	75% (2000)	[8]
rGO@HM-ZMO	116.7 (0.1 A g^{-1})	39.1% (0.1 to 2 A g^{-1})	No negligible	[9]
ZnMn$_2$O$_4$	190.4 (0.2 A g^{-1})	32.6% (0.2 to 6.4 A g^{-1})	94.4% (500)	[10]
ZnMn$_2$O$_4$@N-rGO	204.4 (0.01 A g^{-1})	32.2% (0.01 to 1.5 A g^{-1})	84.7% (600)	[11]
OD-ZMO@PEDOT	221 (0.083 A g^{-1})	28.3% (0.083 to 1.66 A g^{-1})	93.8% (300)	[12]
ZnMn$_2$O$_4$/Mn$_2$O$_3$	130 (0.1 A g^{-1})	22.3% (0.1 to 6.4 A g^{-1})	No negligible	[13]

References

1   Z. Yao, D. Cai, Z. Cui, Q. Wang and H. Zhan, *Ceram. Int.*, 2020, **46**, 11237.

2   S. Islam, M.H. Alfaruqi, D.Y. Putro, S. Park, S. Kim, S. Lee, M.S. Ahmed, V. Mathew, Y.K. Sun and J.Y. Hwang, *Adv. Sci.*, 2021, **8**, 2002636.

3   X. Wu, Y. Xiang, Q. Peng, X. Wu, Y. Li, F. Tang, R. Song, Z. Liu, Z. He and X. Wu, *J. Mater. Chem. A*, 2017, **5**, 17990.

4   M. Shi, B. Wang, Y. Shen, J. Jiang, W. Zhu, Y. Su, M. Narayanasamy, S.

Angaiah, C. Yan and Q. Peng, *Chem. Eng. J.*, 2020, 399, 125627.

5 N. Zhang, F. Cheng, Y. Liu, Q. Zhao, K. Lei, C. Chen, X. Liu and J. Chen, *J. Am. Chem. Soc.*, 2016, **138**, 12894.

6 C. Yang, M. Han, H. Yan, F. Li, M. Shi and L. Zhao, *J. Power Sources*, 2020, **452**, 227826.

7 V. Soundharrajan, B. Sambandam, S. Kim, S. Islam, J. Jo, S. Kim, V. Mathew, Y.-k. Sun, J. Kim, *Energy Storage Mater.*, 2020, **28**, 407.

8 T.H. Wu, and W.Y. Liang, *ACS Appl. Mater. Interfaces*, 2021, **13**, 23822.

9 L. Chen, Z. Yang, H. Qin, X. Zeng, J. Meng and H. Chen, *Electrochim. Acta*, 2019, **317**, 155.

10 L. Yan, X. Zeng, Z. Li, X. Meng, D. Wei, T. Liu, M. Ling, Z. Lin and C. Liang, *Mater. Today Energy*, 2019, **13**, 323.

11 Y. Tao, Z. Li, L. Tang, X. Pu, T. Cao, D. Cheng, Q. Xu, H. Liu, Y. Wang and Y. Xia, *Electrochim. Acta*, 2020, **331**, 135296.

12 H. Zhang, J. Wang, Q. Liu, W. He, Z. Lai, X. Zhang, M. Yu, Y. Tong and X. Lu, *Energy Storage Mater.*, 2019, **21**, 154.

13 S. Yang, M. Zhang, X. Wu, X. Wu, F. Zeng, Y. Li, S. Duan, D. Fan, Y. Yang, X. Wu, *Electroanaly. Chem.*, 2019, **832**, 69.